


# High SQLE Expression and Gene Amplification Correlates with Poor Prognosis in Head and Neck Squamous Cell Carcinoma

Yang Liu

Lijun Fang\*

Weixian Liu \*

Department of Oral Surgery, Shengjing Hospital of China Medical University, Shenyang, Liaoning Province, People's Republic of China

\*These authors contributed equally to this work

**Objective:** Squalene epoxidase (SQLE) is considered a metabolic oncogene, but its biological function and prognostic value in head and neck squamous cell carcinoma (HNSCC) remain unclear. We aimed to evaluate the role of SQLE in the occurrence and development of HNSCC through bioinformatics analysis, and validation experiments.

**Methods:** Transcriptomic, genomic, and clinical data from The Cancer Genome Atlas were used for pan-cancer analysis. SQLE expression in HNSCC was evaluated using Gene Expression Omnibus datasets and immunohistochemistry. The biological significance of SQLE in the tumor microenvironment (TME) of HNSCC was determined using TISCH, HuRI, LinkedOmics, and TIMER 2.0. The prognostic value of SQLE in HNSCC was analyzed using univariate Cox regression and Kaplan–Meier survival curves. Effect of SQLE on the Cal27 HNSCC cell line was evaluated using cell counting kit 8, wound healing, and EdU assays.

**Results:** SQLE was overexpressed and amplified in various cancers, including HNSCC. High SQLE expression promoted cell proliferation, associated with T stage in HNSCC patients. Copy number amplification and DNA demethylation contributed to high SQLE expression in HNSCC, which was associated with poor prognosis. SQLE was related to HNSCC TME, and its mRNA expression/copy number alterations were negatively correlated with the infiltration of CD8+ T cells, follicular helper T cells, and regulatory T cell infiltration and mast cell activation and positively correlated with the infiltration of M0 macrophages and resting mast cells in HNSCC.

**Conclusion:** SQLE was identified as a prognostic biomarker and a potential pharmaceutical target for HNSCC.

**Keywords:** copy number amplification, DNA methylation, head and neck squamous cell carcinoma, immune cell infiltration, multi-omics analysis, squalene epoxidase

## Introduction

Globally, more than 800,000 new cases and 500,000 deaths associated with head and neck cancer have been reported annually.<sup>1</sup> This disease has a huge impact on the function and aesthetics of patients and reduces their quality of life.<sup>2</sup> Head and neck cancer is one of the most common malignant tumors worldwide, and squamous cell carcinoma is the main pathological type. Head and neck squamous cell carcinoma (HNSCC) mainly occurs in the oral cavity, pharynx, and larynx and is closely related to tobacco and alcohol consumption and human papillomavirus infection.<sup>3</sup> Despite continuous developments in the treatment methods for HNSCC, such as surgery,

Correspondence: Weixian Liu; Lijun Fang  
Email liuweixiansj@163.com; fanglj@sj-hospital.org

chemoradiotherapy, and immunotherapy, the survival rate has not significantly improved.<sup>4</sup> Therefore, identifying new therapeutic targets for HNSCC is of great significance to better understand disease pathogenesis and to develop new therapeutic methods.

Cholesterol plays a crucial role in several important aspects of the maintenance of cell life, including cell proliferation and differentiation, membrane biogenesis, and molecular and vesicular transport.<sup>5</sup> The acquisition of oncogenes and the loss of tumor suppressor genes lead to the production of cancer cells and reprogramming of the cholesterol metabolism pathway.<sup>6</sup> Increasing evidence shows that abnormal cholesterol metabolism is widespread in a variety of carcinogenic processes and promotes the progression of cancer. Accordingly, cholesterol accumulation has been reported in oral squamous cell carcinoma, clear-cell renal carcinoma, prostate cancer, and breast cancer.<sup>7–10</sup>

Squalene epoxidase (SQLE) is a monooxygenase that catalyzes the conversion of squalene to 2,3(S)-oxidosqualene.<sup>11</sup> SQLE is the second rate-limiting enzyme in the cholesterol synthesis pathway, and its inhibition effectively reduces cholesterol synthesis.<sup>12</sup> For a long time, it has been known that SQLE is highly amplified in a variety of cancers and drives abnormal metabolism; thus, it is considered a metabolic oncogene.<sup>13</sup> The overexpression of SQLE has been shown to promote the proliferation and metastasis of lung squamous cell carcinoma, hepatocellular carcinoma, and esophageal squamous cell carcinoma<sup>14–16</sup> and is associated with poor prognosis of prostate cancer and breast cancer.<sup>17,18</sup> Another study identified a subset of neuroendocrine tumors, especially small cell lung cancers, showing significant sensitivity to the inhibition of SQLE.<sup>19</sup> At present, the catalytic domain of human SQLE has been identified, which provides the possibility of the rational development of new targeted drugs.<sup>20,21</sup> However, the biological mechanism of SQLE in HNSCC has not been systematically elucidated. Therefore, this study aimed to evaluate the role of SQLE in the occurrence and development of HNSCC horizontally and vertically through pan-cancer analysis, multi-omics analysis, and validation experiments.

## Materials and Methods

### Data Extraction and Processing

The raw data of GSE30784, GSE13601, GSE33205, and GSE9844 datasets were downloaded from the Gene Expression Omnibus (GEO) database (<http://ncbi.nlm.nih.gov/geo>), including 268 HNSCC samples and 108 normal

samples. The microarray data from CEL files were pre-processed using the Robust Multi-Array Average algorithm of the R package *affy* for background correction, quantile normalization, and log<sub>2</sub> transformation. RNA-sequencing data and clinical data of 9736 tumor samples and 8587 normal samples based on The Cancer Genome Atlas (TCGA) and GTEx projects were downloaded from UCSC Xena (<http://xena.ucsc.edu>). TCGA pan-cancer mutation and copy number alterations (CNAs) data were downloaded from cBioPortal ([www.cbioportal.org](http://www.cbioportal.org)). Methylation data of the TCGA-HNSC cohort were obtained by the shiny methylation analysis resource tool<sup>22</sup> (<http://www.bioinfo-zs.com/smartapp>).

### Tumor Immune Single-Cell Hub (TISCH)

TISCH<sup>23</sup> (<http://tisch.comp-genomics.org>) is a scRNA-seq database, which aims to characterize the tumor microenvironment at single-cell resolution and adopt a uniform analysis pipeline to perform quality control, clustering, and cell-type annotation for each collected dataset. GSE103322 is a primary HNSCC dataset of TISCH; it contains data from 5902 single cells from 18 patients. The expression of SQLE in different cell types based on the GSE103322 dataset was visualized using TISCH.

### Protein–Protein Interaction (PPI) Network

A PPI network was constructed based on PPI data from The Human Reference Protein Interactome Mapping Project<sup>24</sup> (HuRI, <http://www.interactome-atlas.org>), which provides the largest reference map of human binary protein interactions to date using high-throughput yeast two-hybrid screens to detect PPIs systematically. SQLE was the hub gene of the PPI network, and gene set enrichment analysis of all interactors was performed with Metascape<sup>25</sup> (<http://metascape.org>).

### LinkedOmics

LinkedOmics<sup>26</sup> (<http://www.linkedomics.org>) is a public web portal containing multi-omics data from all 32 TCGA cancer types. The web application has three analytical modules: LinkFinder, LinkInterpreter, and LinkCompare. First, genes co-expressed with SQLE in the TCGA-HNSC cohort were identified from the LinkFinder module, and Pearson correlations were performed. Then, the LinkInterpreter module was used to perform enrichment analysis of co-expressed genes based on Gene Ontology (GO) and Kyoto Encyclopedia of Genes and Genomes (KEGG) pathway analyses.

## Timer 2.0

The correlation between the expression and copy number alterations of SQLE and immune infiltrates was explored using TIMER 2.0<sup>27</sup> (<http://timer.cistrome.org/>), which is a comprehensive resource for the systematic analysis of immune infiltrates across diverse cancer types. Immune infiltration estimations were performed based on CIBERSORT algorithms. Spearman rank correlation was used.

## Patients and Tissue Specimens

Forty primary HNSCC tumor samples and 15 adjacent normal tissue samples were collected from the Department of Pathology at Shengjing Hospital of China Medical University from January 2015 to December 2016. All patients had no history of chemotherapy or radiotherapy. The differentiation degree and tumor–nodes–metastases stage of HNSCC were determined according to The American Joint Committee on Cancer Staging Manual (8th Edition). All research protocols were approved by the hospital ethics committee.

## Cell Culture

The human HNSCC cell line Cal27 was purchased from Cell Bank of the Chinese Academy of Sciences (Beijing, China) and cultured in Dulbecco's modified Eagle's medium (DMEM, Hyclone, Beijing, China) with 1% penicillin-streptomycin and 10% fetal bovine serum (GIBCO, New York, NY, USA). All cells were cultured in humidified air containing 5% CO<sub>2</sub> at 37 °C.

## Immunohistochemistry (IHC)

IHC was performed according to SP kit instructions (SP-9000; ZSGB-BIO, Beijing, China). Briefly, 4-μm tissue sections were heated in citrate buffer in a microwave oven for 20 min for antigen repair after dewaxing and hydration. Next, the sections were incubated with an endogenous peroxidase blocker at room temperature for 15 min and then blocked in 5% goat serum for 30 min at 37 °C. Subsequently, the blocked tissue sections were incubated overnight at 4 °C with an anti-SQLE rabbit polyclonal antibody (1:200; Proteintech, Wuhan, China), followed by further incubation with secondary antibodies for 30 min at 37 °C. As a negative control, phosphate-buffered saline (PBS) was used instead of the SQLE antibody. Proteins were visualized using a 3,3'-diaminobenzidine solution kit (ZSGB-BIO, Beijing, China). Finally, sections were observed under a light microscope and evaluated based on the immune response score (IRS), which

was multiplied by the staining proportion score (PS) and staining intensity score (IS). PS was defined as 0 (0%), 1 (1%–33%), 2 (33%–66%), and 3 (66%–100%). IS was divided into 0 (negative), 1 (weak), 2 (moderate), and 3 (strong). According to IRS, patients were divided into three groups as follows: negative expression group, IRS = 0; weak expression group, IRS = 1–3; and strong positive expression group, IRS 4–9. All sections were independently scored by two pathologists blinded to the clinicopathological features and clinical data of the cohort.

## Western Blotting

Collected cells were lysed in RIPA buffer (Solarbio, Beijing, China) for 30 min on ice and centrifuged at 14,000 xg for 10 min for collecting the total protein samples. Next, the samples were separated by 10% sodium dodecyl sulphate-polyacrylamide gel electrophoresis. Resolved proteins were transferred to polyvinylidene difluoride membranes (Solarbio, Beijing, China). The membranes were blocked in 5% skim milk for 2 h and then incubated overnight with an anti-SQLE rabbit polyclonal antibody (1:1000; Proteintech, Wuhan, China) at 4 °C. The next day, the membranes were incubated with a secondary antibody. Finally, according to the manufacturer's instructions, an enhanced ECL luminescence detection kit (Vazyme, Nanjing, China) was used to observe the protein bands on the membranes.

## RNA Interference

Small interfering RNA (siRNA) and scrambled siRNA targeting SQLE were designed and synthesized by GenePharma (Shanghai, China). The siRNA sequences used to target SQLE were 5'-GCCGGGUGGUUAUCAUGUUTT-3' and 5'-AACAUGAUAAACCACCCGGCTT-3'. All these siRNAs were transfected into cells with Lipofectamine 3000 (Invitrogen, San Diego, CA, USA) according to the manufacturer's instructions. The knockdown efficiency was determined after 48 h of culture.

## Cell Proliferation Assay

Cell counting kit-8 (CCK-8; GLPBIO, Montclair, USA) was used to detect cell proliferation. After 18–24 h of transfection, Cal27 cells were seeded onto 96-well plates ( $4 \times 10^3$  cells/well). After 24, 48, and 72 h of culture, 100 μL of fresh medium containing 10% CCK-8 reagent was added to each well, and then, cells were cultured at 37 °C in 5% CO<sub>2</sub> for 2 h. The optical density at 450 nm was detected with a microplate reader (BioTek Instruments, Winooski, USA).

Moreover, cell proliferation was detected through the 5-ethynyl-2'-deoxyuridine (EdU) proliferation assay. After 18–24 h of transfection, EdU was added to the 6-well plates, and the cells were cultured for an extra 2 h. Next, the proliferation rate of the cells was assessed with BeyoClick™ EDU-488 (Beyotime, Shanghai, China) following the manufacturer's instructions. Five randomly selected regions were examined with a fluorescence microscope (Olympus, Tokyo, Japan) to analyze the proliferation rate.

## Cell Migration Assay

Wound healing tests were performed to evaluate cell migration. Once transfected cells were cultured to 95% confluence in 6-well plates, a wound was made across cell monolayers with a 100  $\mu$ L pipette tip. The floating cells were washed with PBS, and then, serum-free DMEM was added. After 24 h, wound healing was photographed.

## Statistical Analysis

Statistical analysis was performed with R software (R version 3.5.0) or GraphPad Prism 8 (GraphPad Software, CA, USA) using Student's *t* test,  $\chi^2$  test, Kruskal–Wallis test, or one-way analysis of variance, as appropriate. Prognostic parameters were estimated with univariate Cox regression analysis. A Kaplan–Meier survival curve was used for survival analysis. Pearson correlation or spearman rank correlation test was used for correlation analyses. All experiments were performed in triplicate, unless otherwise specified, and the results are presented as the mean  $\pm$  standard deviation.

## Results

### Transcriptome Level, Somatic Mutations, Copy Number Alterations, and Prognostic Value of SQLE in Pan-Cancer Cohorts

RNA-seq data of 9736 tumor samples and 8587 normal samples showed that SQLE mRNA expression was significantly upregulated in 21 cancers including HNSCC ( $P < 0.001$ ) and downregulated in 6 cancers ( $P < 0.001$ ) (Figure 1A). Among 11,317 patients in the TCGA Pan-cancer cohorts, only 38 had SQLE somatic mutations, and the overall mutation frequency was less than 0.1%. At the copy number level, deep deletion occurred in four cases and high amplification occurred in 954 cases. The total copy number alteration frequency was 8.47%. The top five cancers with the highest copy number amplification frequency were ovarian carcinoma (36.44%, 211/579),

esophageal carcinoma (20.65%, 38/184), breast invasive carcinoma (18.8%, 203/1080), liver hepatocellular carcinoma (17.84%, 65/370) and uveal melanoma (17.5%, 14/80). For the cancers with SQLE overexpression, except DLBC, all other cancers had copy number amplifications of SQLE, with the amplification frequency ranging from 0.81% to 36.44% (Figure 1B). Therefore, copy number amplification plays an important role in the upregulation of SQLE mRNA expression in multiple cancers.

Then, univariate Cox regression analysis was used to evaluate the prognostic value of SQLE mRNA expression in the TCGA Pan-cancer cohorts, which showed that SQLE mRNA expression was a high-risk factor for overall survival (OS) of bladder urothelial carcinoma (HR=1.2; 95% CI, 1.04–1.39;  $P=0.014$ ), breast invasive carcinoma (HR=1.17; 95% CI, 1.02–1.36;  $P=0.029$ ), cervical squamous cell carcinoma (HR=1.3; 95% CI, 1.05–1.62;  $P=0.017$ ), head and neck squamous cell carcinoma (HR=1.24; 95% CI, 1.06–1.45;  $P=0.008$ ), kidney renal clear cell carcinoma (HR=1.3; 95% CI, 1.04–1.63;  $P=0.023$ ), kidney renal papillary cell carcinoma (HR=1.66; 95% CI, 1.35–2.05;  $P < 0.001$ ), lung adenocarcinoma (HR=1.16; 95% CI, 1.01–1.33;  $P=0.038$ ), mesothelioma (HR=1.75; 95% CI, 1.31–2.35;  $P < 0.001$ ), pancreatic adenocarcinoma (HR=1.35; 95% CI, 1.09–1.67;  $P=0.006$ ), sarcoma (HR=1.5; 95% CI, 1.25–1.8;  $P < 0.001$ ), thyroid carcinoma (HR=2.19; 95% CI, 1.12–4.27;  $P=0.021$ ), and uterine corpus endometrial carcinoma (HR=1.24; 95% CI, 1.00–1.54;  $P=0.046$ ), uveal melanoma (HR=2.11; 95% CI, 1.48–3.01;  $P < 0.001$ ) (Figure 1C). Moreover, SQLE was a high-risk factor for the progression-free survival (PFS) of adrenocortical carcinoma (HR=1.23; 95% CI, 1.02–1.48;  $P=0.027$ ), bladder urothelial carcinoma (HR=1.23; 95% CI, 1.08–1.4;  $P=0.001$ ), cervical squamous cell carcinoma (HR=1.23; 95% CI, 1.01–1.5;  $P=0.041$ ), head and neck squamous cell carcinoma (HR=1.24; 95% CI, 1.08–1.43;  $P=0.003$ ), kidney renal clear cell carcinoma (HR=1.22; 95% CI, 1.01–1.49;  $P=0.043$ ), kidney renal papillary cell carcinoma (HR=1.37; 95% CI, 1.14–1.63;  $P < 0.001$ ), mesothelioma (HR=1.53; 95% CI, 1.17–2;  $P=0.002$ ), pancreatic adenocarcinoma (HR=1.33; 95% CI, 1.1–1.62;  $P=0.003$ ), sarcoma (HR=1.28; 95% CI, 1.11–1.48;  $P < 0.001$ ), thyroid carcinoma (HR=1.45; 95% CI, 1.01–2.08;  $P=0.047$ ), and uterine corpus endometrial carcinoma (HR=1.24; 95% CI, 1.06–1.46;  $P=0.009$ ), uveal melanoma (HR=2.24; 95% CI, 1.64–3.04;  $P < 0.001$ ) (Figure 1D). Notably, the high expression of SQLE was significantly associated with poor OS and PFS in TCGA-HNSC cohorts.



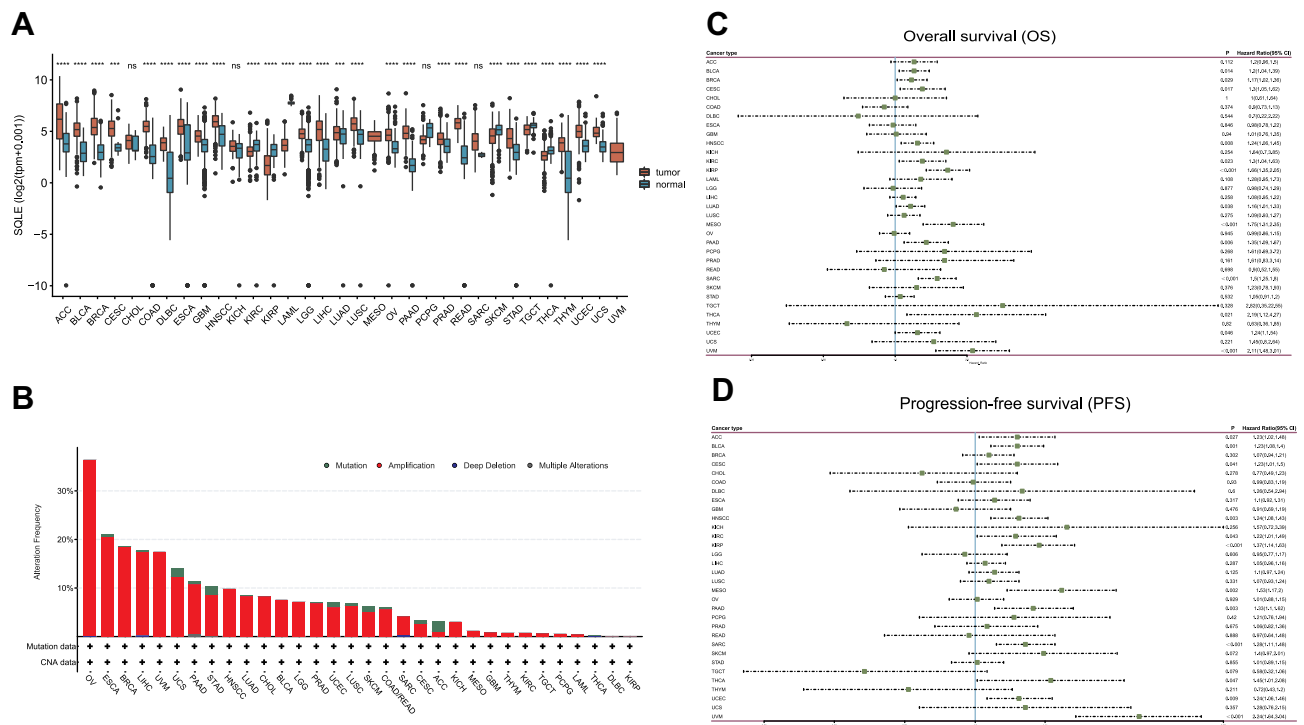


**Figure 1** Transcriptome level, somatic mutations, copy number alterations, and prognostic value of SQLE in pan-cancer cohorts. **(A)** SQLE mRNA expression in different cancer types from TCGA and GTEx data. (\*\* $P < 0.001$ , \*\*\* $P < 0.0001$ ) **(B)** Alteration frequency of SQLE gene in different cancers obtained from the cBioPortal. **(C)** The correlation between SQLE mRNA expression and overall survival in TCGA pan-cancer cohorts using univariate Cox regression analysis. **(D)** The correlation between SQLE mRNA expression and progression-free survival in TCGA pan-cancer cohorts using univariate Cox regression analysis.

## SQL Expression in HNSCC

The differential SQLE mRNA expression in HNSCC was further verified based on four independent datasets (GSE30784, GSE13601, GSE33205, and GSE9844), which revealed that SQLE mRNA expression in HNSCC was significantly higher than that in normal tissues ( $P < 0.001$ ) (Figure 2A). In addition, the scRNA-seq dataset GSE103322 was used to explore SQLE mRNA expression in the HNSCC microenvironment (Figure 2B). As shown in the cluster and violin diagrams (Figure 2C and D), SQLE was highly expressed in malignant cells but rarely expressed in nonmalignant cells (including stromal and immune cells). Therefore, the overexpression of SQLE mRNA in HNSCC was mainly attributed to cancer cells, rather than to stromal and immune cells.

To confirm the difference of SQLE protein expression in HNSCC, 40 primary tumor samples and 15 adjacent normal samples were analyzed by IHC. The results showed that SQLE protein was primarily detected in the tumor cell cytoplasm (magnification,  $\times 200$ ) and the positive expression rate of SQLE in primary HNSCC was 100% (40/40), of which 27.50% (11/40) were low expression samples and

72.50% (29/40) were high expression samples. However, the positive expression rate in normal tissues was 53.33% (8/15). Consequently, the expression of SQLE protein in HNSCC was significantly higher than that in normal tissues ( $P<0.001$ ) (Figure 2E–H). Moreover, the upregulated protein expression of SQLE was significantly associated with T stage ( $P=0.0108$ ) of HNSCC (Table 1).

## Overexpression of SQLE is Associated with Poor Prognosis of Patients with HNSCC

Univariate Cox regression analysis showed that high expression of SQLE is a high-risk factor for OS and PFS of patients with HNSCC. Then, 499 TCGA-HNSC patients with OS and PFS data were divided into high-SQLE (n = 249) and low-SQLE (n = 250) expression groups. Kaplan–Meier curve and log rank test showed that high SQLE expression was significantly associated with poor OS of patients with HNSCC ( $P=0.0017$ ) (Figure 3A). In addition, the PFS of patients with HNSCC with high SQLE expression was significantly worse ( $P=0.00039$ ) (Figure 3B).

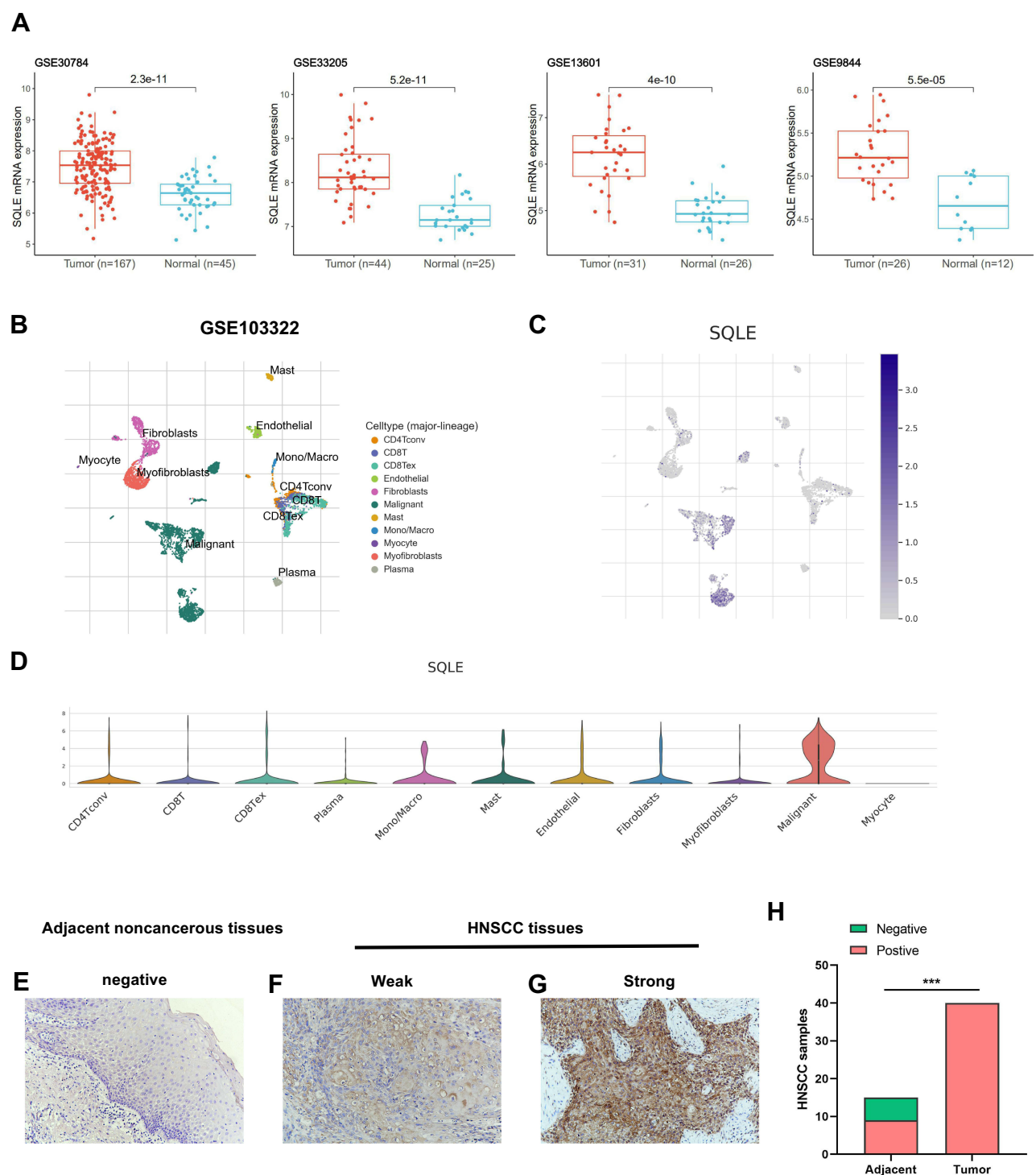


**Figure 2** SQLE expression in HNSCC. **(A)** Differential SQLE mRNA expression between HNSCC and normal tissues of four independent datasets (GSE30784, GSE13601, GSE33205, and GSE9844). **(B)** Clusters and cell-type annotation (major-lineage) of GSE103322. **(C)** UMAP plot presenting SQLE mRNA expression in differential cell types of HNSCC TME. **(D)** Violin plot presenting SQLE mRNA expression in differential cell types of HNSCC TME. **(E–H)** SQLE protein expression in tissues were determined by IHC staining. (magnification 200×). P-values are based on chi-squared or Fisher's exact test.  $P < 0.05$  indicates a significant association among the variables. (\*\*\*)  $P < 0.001$ .

**Table I** Association Between SQLE Protein Expression and Clinicopathological Features

| Characteristics   | n(40) | Low SQLE Expression (n=11) | High SQLE Expression (n=29) | P-value |
|-------------------|-------|----------------------------|-----------------------------|---------|
| <b>Age(years)</b> |       |                            |                             | 0.0602  |
| <60               | 24    | 4                          | 20                          |         |
| ≥60               | 16    | 7                          | 9                           |         |
| <b>Sex</b>        |       |                            |                             | 0.6638  |
| Female            | 13    | 3                          | 10                          |         |
| Male              | 27    | 8                          | 19                          |         |
| <b>T stage</b>    |       |                            |                             | 0.0108* |
| T1/T2             | 28    | 11                         | 17                          |         |
| T3/T4             | 12    | 0                          | 12                          |         |
| <b>N stage</b>    |       |                            |                             | 0.8159  |
| N0                | 23    | 6                          | 17                          |         |
| N1/N2             | 17    | 5                          | 12                          |         |
| <b>AJCC stage</b> |       |                            |                             | 0.5826  |
| I/II              | 19    | 6                          | 13                          |         |
| III/IV            | 21    | 5                          | 16                          |         |
| <b>Grade</b>      |       |                            |                             | 0.2082  |
| G1                | 19    | 7                          | 12                          |         |
| G2/G3             | 21    | 4                          | 17                          |         |
| <b>Location</b>   |       |                            |                             | 0.3434  |
| Lips              | 3     | 0                          | 3                           |         |
| Gingiva           | 8     | 1                          | 7                           |         |
| Tongue            | 16    | 7                          | 9                           |         |
| Buccal            | 3     | 1                          | 2                           |         |
| Floor of mouth    | 10    | 2                          | 8                           |         |

**Notes:** P-values are based on chi-squared or Fisher's exact test.  $P < 0.05$  indicates a significant association among the variables. (\* $P < 0.05$ ).

## Copy Number Amplification and DNA Demethylation Synergistically Promote the Overexpression of SQLE in HNSCC

Among 514 TCGA-HNSC patients with complete genomic data, there was no case of an SQLE somatic mutation. According to the putative copy number alterations from GISTIC, 514 patients were divided into four groups (shallow deletion,  $n = 4$ ; diploid,  $n = 133$ ; gain,  $n = 326$ ; and amplification,  $n = 51$ ), and SQLE mRNA expression in the diploid, gain, and amplification groups was found to increase in a gradient-dependent manner ( $P < 0.001$ ) (Figure 4A); the sample size of the shallow deletion group was too small to be included in the statistics. Moreover, we evaluated the association between SQLE copy number alterations and 5-year OS. As shown by the Kaplan–Meier curve (Figure 4B), increased SQLE copy number was associated with shorter 5-year OS of TCGA-HNSC patients ( $P < 0.05$ ). These results indicated that

SQLE mRNA expression was upregulated with an increase in copy number in HNSCC.

To further explore the mechanism underlying SQLE overexpression, we continued to evaluate the DNA methylation level of SQLE in the TCGA-HNSC cohort. Ten methylation sites (CpGs) in SQLE were detected by Illumina Infinium HumanMethylation 450 Beadchip, among which cg02553489, cg04618607, cg12108029, cg12267291, cg16688232, and cg21894883 were located in Island; cg22011731, cg09984392, and cg14660676 were located in S<sub>2</sub> Shore; and cg23587955 was located in Opensea (Figure 5A). The methylation levels (beta value) of three CpG sites in S<sub>2</sub> Shore were significantly lower in tumor tissues than in normal tissues ( $P < 0.001$ ) (Figure 5B), suggesting that SQLE was significantly demethylated in HNSCC. In addition, the methylation levels of cg02553489, cg04618607, cg12108029, cg16688232, cg21894883, cg22011731, cg09984392, and cg14660676 were negatively correlated with SQLE mRNA expression ( $P < 0.001$ ) (Figure 5C). Notably, the methylation

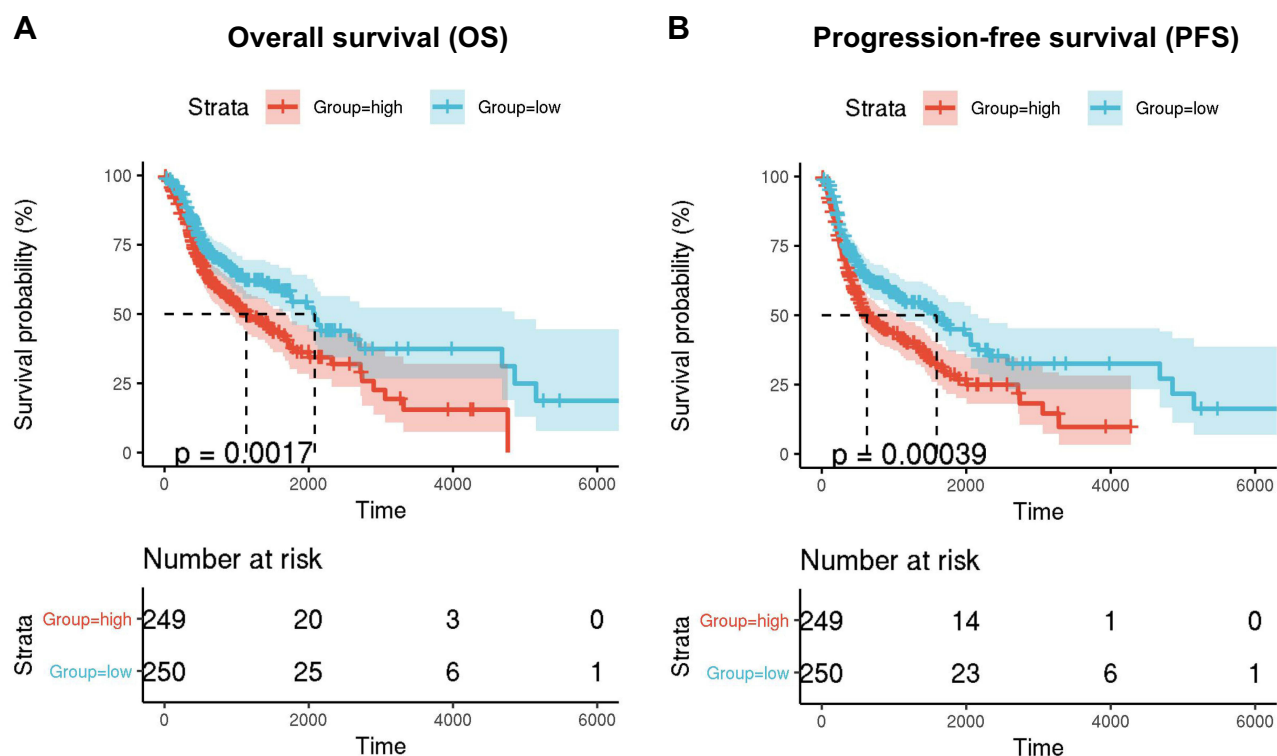


**Figure 3** Kaplan-Meier survival curves comparison of high and low mRNA expression of SQLE. (A) Overall survival (OS) (B) progression-free survival (PFS).

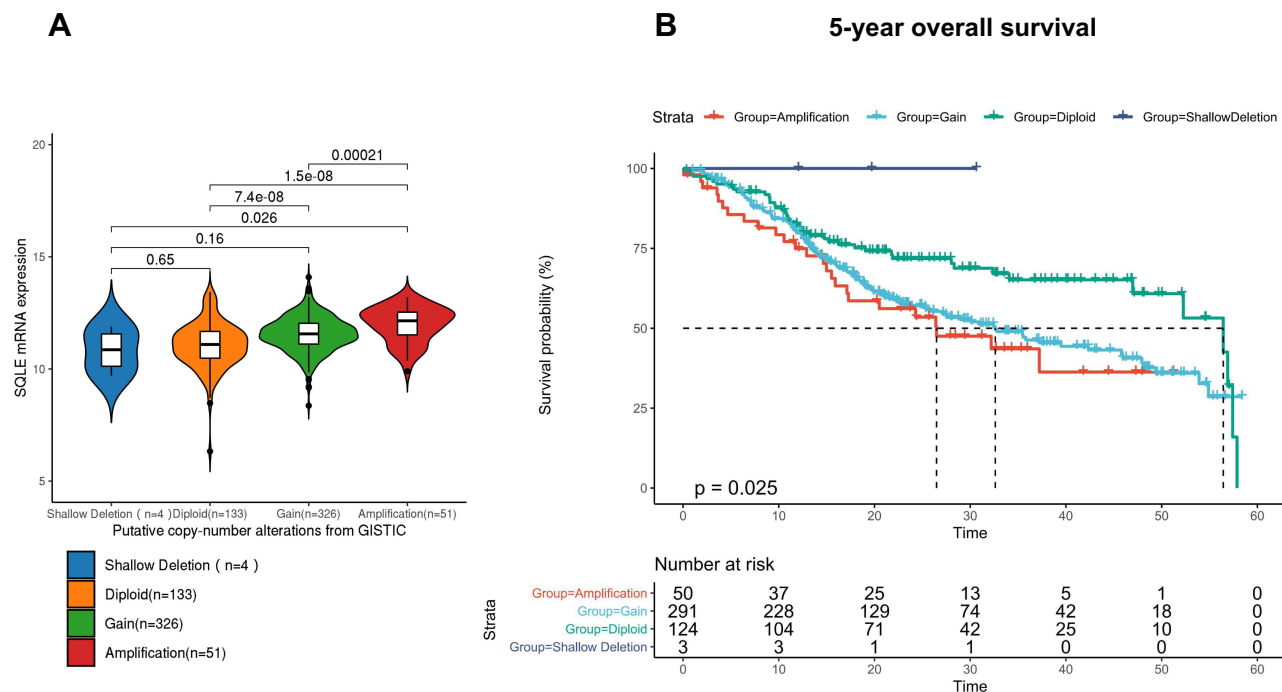


**Figure 4** Copy number alterations in TCGA-HNSC cohort. (A) SQLE mRNA expression in different copy number alteration groups. (B) 5-year overall survival of different copy number alteration groups.

level of cg14660676 not only had the strongest correlation with SQLE mRNA expression among all CpGs ( $R=-0.42$ ,  $P<2.2e-16$ ) but also showed a significant downward trend

with an increase in the SQLE copy number ( $P<0.001$ ) (Figure 5D). In general, demethylation of cg14660676 promotes SQLE mRNA overexpression in HNSCC.



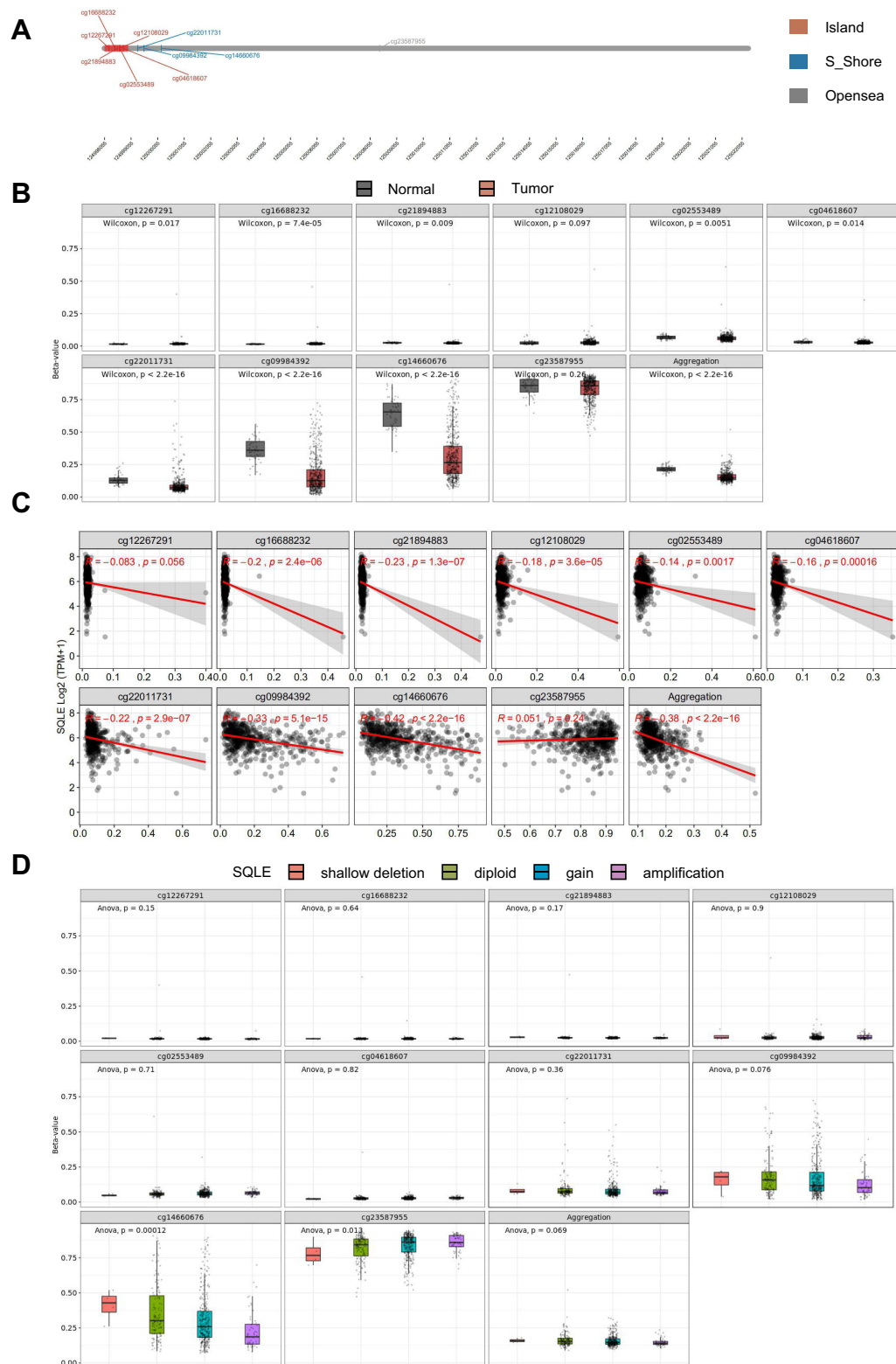


**Figure 5** SQLE methylation levels in TCGA-HNSC cohort. **(A)** Chromosomal distribution of the methylation probes associated with SQLE. **(B)** Comparison of SQLE methylation value between normal and tumor samples. **(C)** Correlation between SQLE mRNA expression and methylation. **(D)** SQLE methylation value with copy number alterations.

## Identification of SQLE PPI Network and Co-Expressed Genes in HNSCC

The map of HuRI showed that SQLE could directly interact with REEP4, TMEM14B, and CREB3L1 and that REEP4, TMEM14B, and CREB3L1 could interact with 102, 230, and 189 proteins, respectively, all of which form a complex PPI network (Figure 6A). According to the results of the enrichment analysis of interactors using Metascape (Figure 6B), the PPI network involved many pathways related to cholesterol metabolism, such as

SNARE interactions in vesicular transport, vascular fusion with Golgi attachments, lipid biological process, and membrane lipid metabolic processes. Of note, 21 proteins were involved in the regulation of leucocyte migration.

To further explore the biological significance of SQLE in HNSCC, the LinkFinder module of LinkedOmics was applied to analyze the genes co-expressed with SQLE in 520 TCGA-HNSC samples. As shown in the volcanic map (Figure 6C), 564 genes were positively correlated with SQLE mRNA expression ( $R>0.3$ ,  $P<0.01$ ,  $FDR<0.01$ ), whereas 822 genes

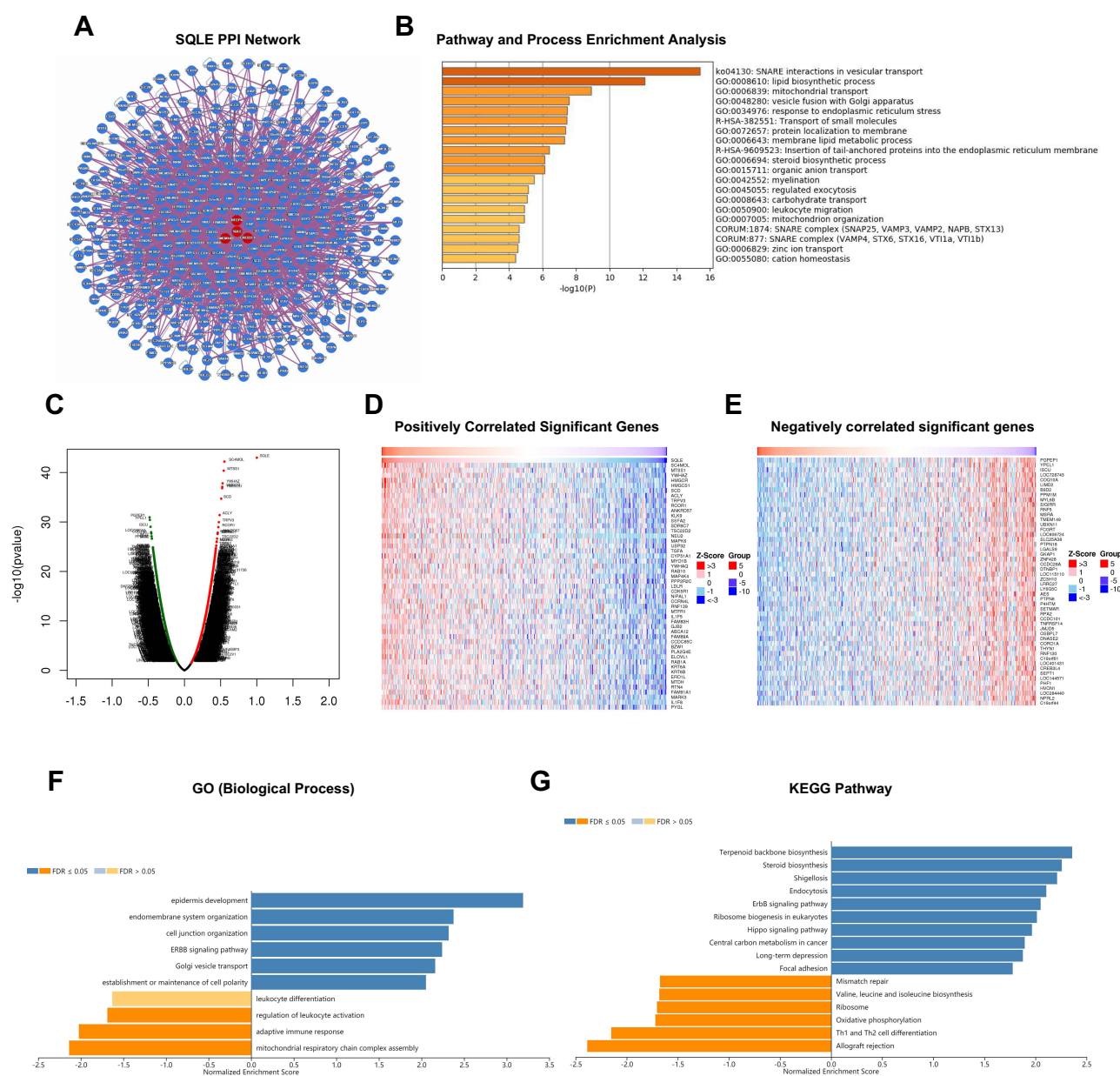


**Figure 6** Identification of SQLE PPI network and co-expressed genes in HNSCC. (A) SQLE PPI network. (B) Enrichment analysis results of interactors associated with PPI network. (C) Correlation between SQLE and co-expressed genes (Pearson test). (D) Top 50 positively correlated significant genes ( $R>0.3$ ,  $P<0.01$ ,  $FDR<0.01$ ). (E) Top 50 negatively correlated significant genes ( $R<0.3$ ,  $P<0.01$ ,  $FDR<0.01$ ). (F and G) Enrichment analysis results of correlated significant genes.

were negatively correlated ( $R<0.3$ ,  $P<0.01$ ,  $FDR<0.01$ ). The heat map showed the top 50 genes with the strongest positive or negative correlation (Figure 6D and E). Next, the LinkInterpreter module was used for Gene Ontology and KEGG pathway analyses of genes co-expressed with SQLE. The results showed that the genes significantly positively correlated with SQLE were mainly enriched in epidermis development, the ErbB signaling pathway, the Hippo signaling pathway, and other cancer-related pathways, whereas the genes significantly negatively correlated were mainly involved in the adaptive immune response, regulation of leucocyte activation, leucocyte activation, Th1 and Th2 cell differentiation, and other immune-related pathways (Figure 6F and G). Combining the results of the enrichment analysis of the PPI network and co-expressed genes, SQLE may play an important role in the immune regulation of HNSCC.

## Correlation Between SQLE and Immune Infiltration in HNSCC

To further understand the function of SQLE in immune infiltration in HNSCC, we adopted the CIBERSORT algorithm in TIMER 2.0 to estimate the correlation between SQLE mRNA expression and the infiltration of 22 immune

cells. The heatmap showed that SQLE mRNA expression was negatively correlated with the infiltration of CD8<sup>+</sup> T cells in 15 cancers and positively correlated with the infiltration of M0 macrophages in 15 cancers (Figure 7A). SQLE mRNA expression in 11 cancers was both significantly correlated with the infiltration of CD8<sup>+</sup> T cells and M0 macrophages. The scatter plot showed six immune cells with the most significant correlation with SQLE mRNA expression in HNSCC (Figure 7B). CD8<sup>+</sup> T cells ( $R=-0.311$ ,  $P=1.55e-12$ ), follicular helper T cells ( $R=-0.27$ ,  $P=1.04e-09$ ), regulatory T cells ( $R=-0.23$ ,  $P=2.41e-07$ ), and activated mast cells ( $R=-0.174$ ,  $P=1.04e-04$ ) were negatively correlated with SQLE mRNA expression, whereas M0 macrophages ( $R=0.287$ ,  $P=8.17e-11$ ) and resting mast cells ( $R=0.205$ ,  $P=4.63e-06$ ) were positively correlated with SQLE mRNA expression. In addition, we explored the relationship between SQLE copy number alterations and these six immune cells (Figure 7C). The results were consistent with those of previous data. With an increase in the SQLE copy number, the infiltration levels of CD8<sup>+</sup> T cells, follicular helper T cells, regulatory T cells, and activated mast cells gradually decreased ( $P<0.01$ ), whereas those of M0

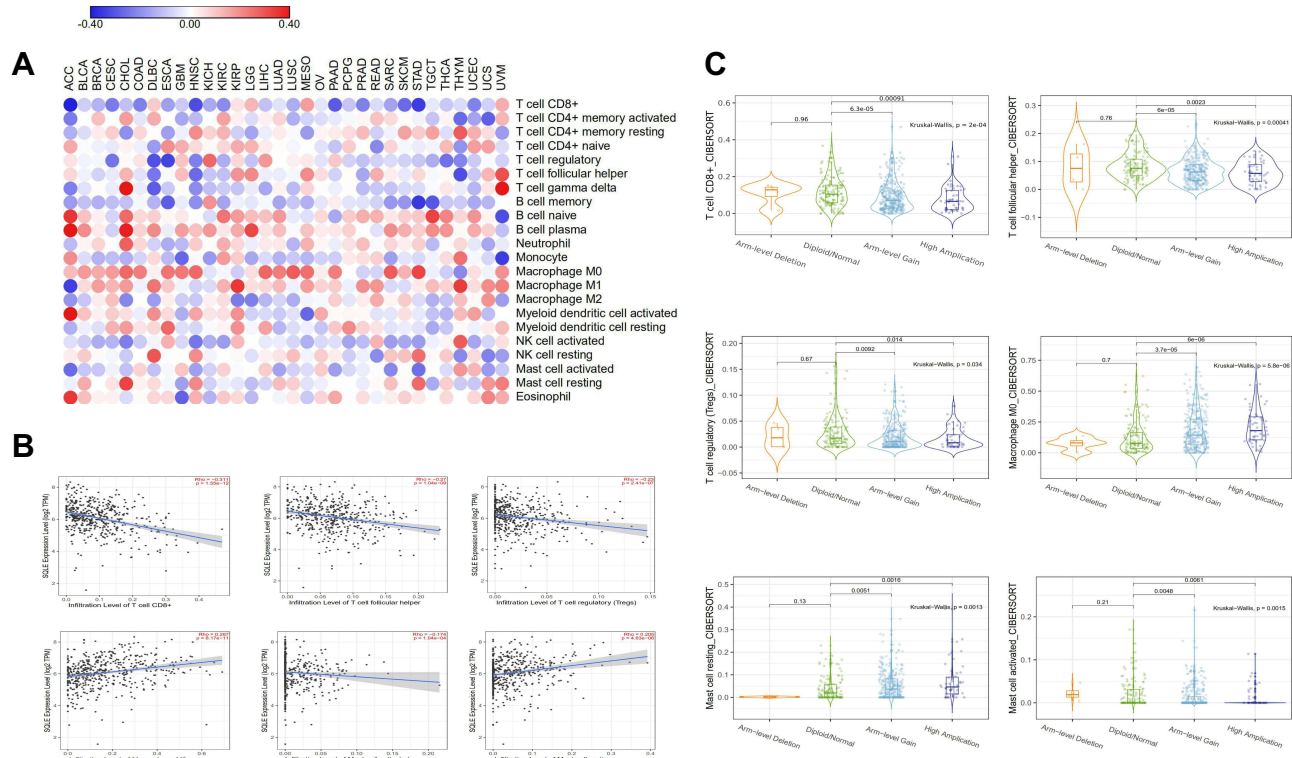


**Figure 7** Correlation between SQLE and immune infiltration in HNSCC. **(A)** Correlation between 22 immune cells infiltration and SQLE mRNA expression in pan-cancer. **(B)** Correlation between 6 immune cells infiltration and SQLE mRNA expression in HNSCC. **(C)** Correlation between 6 immune cells infiltration and SQLE copy number alterations in HNSCC.

macrophages and resting mast cells gradually increased ( $P < 0.01$ ). In general, SQLE may function in the negative immune regulation of HNSCC.

## Knockdown of SQLE Inhibits the Proliferation and Migration of HNSCC Cells in vitro

To evaluate the effect of SQLE on the malignant biological behavior of HNSCC cells, we constructed the SQLE siRNA and transfected it into Cal27 cells. Finally, we observed that SQLE protein expression in Cal27 cells was significantly decreased after transfection (Figure 8A). According to the CCK8 results, SQLE knockdown inhibited the proliferation of Cal27 cells (Figure 8B). In addition, we performed EdU analysis to further confirm these findings. Similarly, the results showed that there were fewer EdU-positive cells in the si-SQLE group and the inhibition of SQLE significantly reduced the number of EdU-positive cells (Figure 8C). In the wound healing test, the migration ability of cells with SQLE knockdown was significantly reduced (Figure 8D). Therefore, SQLE may promote the proliferation and migration of HNSCC cells in vitro.

## Discussion

Recently, it has been reported that the downregulation of SQLE caused by cholesterol accumulation promotes the progression and metastasis of colorectal cancer by activating the  $\beta$ -catenin pathway and inactivating the p53 pathway.<sup>28</sup> In ALK+ anaplastic large cell lymphoma, the loss of SQLE expression results in the accumulation of squalene, which can change the lipid profile and protect cancer cells from ferroptotic cell death.<sup>29</sup> Owing to these findings, the status of SQLE as a cancer driver remains controversial. Similarly, in our pan-cancer analysis, although SQLE was overexpressed and frequently amplified in multiple cancers, it was not associated with poor prognosis in all cancers. For example, SQLE had the highest amplification frequency in ovarian cancer but had no prognostic significance. However, the overexpression of SQLE was significantly correlated with the poor prognosis of HNSCC, which has not been reported before. Therefore, it is very important to clarify the different mechanisms of SQLE in different types of cancer.

Epidermal growth factor receptor (EGFR) is a member of the ErbB family of receptor tyrosine kinases and is overexpressed in more than 90% HNSCC cases.<sup>30</sup> Its downstream signaling pathways include the mitogen-

activated protein kinase signaling pathway and the phosphatidylinositol 3-kinase/Akt signaling pathway,<sup>31</sup> which are crucial for the survival and proliferation of HNSCC.<sup>32</sup> At present, EGFR inhibitors are still the first-line drugs for HNSCC.<sup>33</sup> According to our enrichment analysis of co-expressed genes, the expression of SQLE was positively correlated with the ErbB signaling pathway, which suggested that SQLE plays a prominent role in regulating cell proliferation in HNSCC. Moreover, the role of cholesterol in the survival and growth of cancer cells has received special attention in recent years.<sup>34</sup> Cholesterol synthesis is usually strictly regulated to maintain the balance of intracellular cholesterol metabolism. However, the proliferation of cancer cells is highly dependent on sterol biosynthesis, and deregulation of this pathway can lead to the rapid proliferation and growth of cancer cells.<sup>35</sup> Previous studies have shown that SQLE can promote the proliferation and metastasis of lung squamous cell carcinoma, hepatocellular carcinoma, and esophageal squamous cell carcinoma.<sup>14–16</sup> In addition, an inhibitor of SQLE terbinafine, which is an antifungal agent, has been reported to inhibit the growth of oral squamous cell carcinoma through anti-cancer cell proliferation and anti-angiogenesis mechanisms.<sup>36,37</sup> In this study, SQLE knockdown also significantly inhibited the proliferation of HNSCC cells. Therefore, as a key enzyme in the cholesterol synthesis pathway, SQLE may play an important role in the proliferation and survival of HNSCC.

Abnormal metabolism has always been considered a marker of cancer, but recent discoveries of metabolic reprogramming in the processes of immune cell activation and differentiation have led to the novel concept of “immunometabolism”.<sup>38</sup> Targeting immunometabolism may be a prospective strategy for cancer therapy.<sup>39</sup> Metabolic communication in tumors is involved in tumor immune escape and impacts the TME.<sup>40,41</sup> Tumor-infiltrating immune cells are usually affected by the adverse metabolic activities of tumor cells, resulting in an impaired tumor immune response.<sup>42</sup> Cholesterol is also closely related to the tumor microenvironment. Abnormal metabolism of cholesterol affects various cellular components of the tumor immune microenvironment, including immune cells.<sup>43</sup> CD8+ T cells are the core of anti-tumor immunity.<sup>44</sup> Recent studies have shown that cholesterol negatively regulates IL-9-producing CD8+ T cell differentiation and anti-tumor activity in vivo and in vitro by inducing liver X receptor sumoylation.<sup>45</sup> In addition, the high cholesterol content in the tumor microenvironment of lung cancer disrupts lipid metabolism and increases the ER pressure in



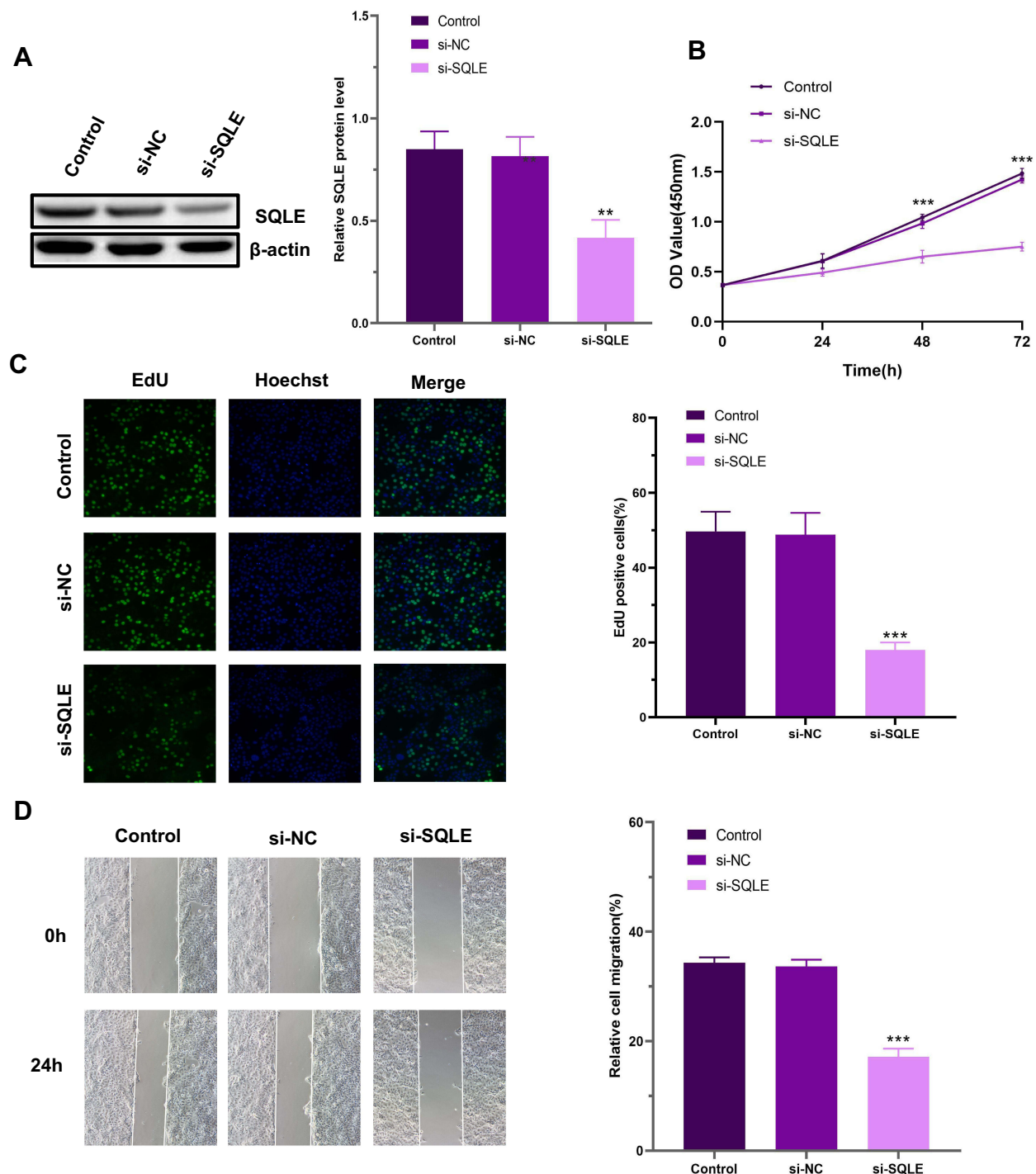


**Figure 8** Knockdown of SQLE inhibits the proliferation and migration of Cal27 cells in vitro. **(A)** The knockdown efficiency was evaluated by Western blotting. **(B)** The CCK8 assay results performed in Cal27 cells. **(C)** Representative images of the EdU assay in Cal27 cells. **(D)** Cell migration was detected by wound healing assay. Each assay was repeated at least three times. Data from one representative experiment is presented as mean  $\pm$  standard deviation. (\*\* $P < 0.01$ , \*\*\* $P < 0.001$ ).

CD8<sup>+</sup> T cells. The ER stress sensor XBP1 regulates the expression of T cell inhibitory receptor, thereby inducing the expression of immune checkpoints of CD8<sup>+</sup> T cells, leading to the depletion of these cells.<sup>46</sup> Although there is no direct

evidence to show the relationship between SQLE and TME immune cell infiltration, it has been reported that SQLE is a key gene for the survival of colorectal and triple receptor negative breast cancers under hypoxic conditions, which

indicates that its overexpression may be related to a hypoxic TME [13]. In this study, we clarified the correlation between SQLE and immune infiltration (especially CD8<sup>+</sup> T cells) in HNSCC based on bioinformatics analysis, but further experiments are needed to explore the specific biological mechanism.

Nevertheless, our results indicate that SQLE could be a prognostic biomarker and a potential pharmaceutical target for HNSCC.

## Data Sharing Statement

All data generated or analyzed during this study are included in this published article.

## Ethics Approval and Consent to Participate

Ethical approval of this study was assessed by the Ethics Committee of Shengjing Hospital of China Medical University. All participants provided written, informed consent and no participants had received any medication prior to sample collection. This study was conducted in accordance with the Declaration of Helsinki.

## Funding

This research did not receive any specific grant from funding agencies in the public, commercial, or not-for-profit sectors.

## Disclosure

The authors declare that they have no known competing financial interests or personal relationships that could have appeared to influence the work reported in this paper.

## References

- Bray F, Ferlay J, Soerjomataram I, Siegel RL, Torre LA, Jemal A. Global cancer statistics 2018: GLOBOCAN estimates of incidence and mortality worldwide for 36 cancers in 185 countries. *CA Cancer J Clin*. 2018;68(6):394–424. doi:10.3322/caac.21492
- Melo Filho MR, Rocha BA, Pires MB, et al. Quality of life of patients with head and neck cancer. *Braz J Otorhinolaryngol*. 2013;79(1):82–88. doi:10.5935/1808-8694.20130014
- Aupérin A. Epidemiology of head and neck cancers: an update. *Curr Opin Oncol*. 2020;32(3):178–186. doi:10.1097/cco.0000000000000629
- Madhukar G, Subbarao N. Current and Future Therapeutic Targets: a Review on Treating Head and Neck Squamous Cell Carcinoma. *Curr Cancer Drug Targets*. 2020;20. doi:10.2174/1568009620666201229120332
- Cirmena G, Franceschelli P, Isnaldi E, et al. Squalene epoxidase as a promising metabolic target in cancer treatment. *Cancer Lett*. 2018;425:13–20. doi:10.1016/j.canlet.2018.03.034
- Xu H, Zhou S, Tang Q, Xia H, Bi F. Cholesterol metabolism: new functions and therapeutic approaches in cancer. *Biochim Biophys Acta Rev Cancer*. 2020;1874(1):188394. doi:10.1016/j.bbcan.2020.188394
- Dickinson A, Saraswat M, Joenväärä S, et al. Mass spectrometry-based lipidomics of oral squamous cell carcinoma tissue reveals aberrant cholesterol and glycerophospholipid metabolism - A Pilot study. *Transl Oncol*. 2020;13(10):100807. doi:10.1016/j.tranon.2020.100807
- Drabkin HA, Gemmill RM. Cholesterol and the development of clear-cell renal carcinoma. *Curr Opin Pharmacol*. 2012;12(6):742–750. doi:10.1016/j.coph.2012.08.002
- Jiang S, Wang X, Song D, et al. Cholesterol Induces Epithelial-to-Mesenchymal Transition of Prostate Cancer Cells by Suppressing Degradation of EGFR through APMAP. *Cancer Res*. 2019;79(12):3063–3075. doi:10.1158/0008-5472.Can-18-3295
- Ehmsen S, Pedersen MH, Wang G, et al. Increased Cholesterol Biosynthesis Is a Key Characteristic of Breast Cancer Stem Cells Influencing Patient Outcome. *Cell Rep*. 2019;27(13):3927–3938. doi:10.1016/j.celrep.2019.05.104
- Yoshioka H, Coates HW, Chua NK, Hashimoto Y, Brown AJ, Ohgane K. A key mammalian cholesterol synthesis enzyme, squalene monooxygenase, is allosterically stabilized by its substrate. *Proc Natl Acad Sci U S A*. 2020;117(13):7150–7158. doi:10.1073/pnas.1915923117
- Zhang C, Zhang H, Zhang M, et al. OSBPL2 deficiency upregulate SQLE expression increasing intracellular cholesterol and cholesterol ester by AMPK/SP1 and SREBF2 signalling pathway. *Exp Cell Res*. 2019;383(2):111512. doi:10.1016/j.yexcr.2019.111512
- Haider S, McIntyre A, van Stiphout RG, et al. Genomic alterations underlie a pan-cancer metabolic shift associated with tumour hypoxia. *Genome Biol*. 2016;17(1):140. doi:10.1186/s13059-016-0999-8
- Ge H, Zhao Y, Shi X, et al. Squalene epoxidase promotes the proliferation and metastasis of lung squamous cell carcinoma cells through extracellular signal-regulated kinase signaling. *Thorac Cancer*. 2019;10(3):428–436. doi:10.1111/1759-7714.12944
- Liu D, Wong CC, Fu L, et al. Squalene epoxidase drives NAFLD-induced hepatocellular carcinoma and is a pharmaceutical target. *Sci Transl Med*. 2018;10:437. doi:10.1126/scitranslmed.aap9840
- Qin Y, Zhang Y, Tang Q, Jin L, Chen Y. SQLE induces epithelial-to-mesenchymal transition by regulating of miR-133b in esophageal squamous cell carcinoma. *Acta Biochim Biophys Sin (Shanghai)*. 2017;49(2):138–148. doi:10.1093/abbs/gmw127
- Stopsack KH, Gerke TA, Andrén O, et al. Cholesterol uptake and regulation in high-grade and lethal prostate cancers. *Carcinogenesis*. 2017;38(8):806–811. doi:10.1093/carcin/bgx058
- Helms MW, Kemming D, Pospisil H, et al. Squalene epoxidase, located on chromosome 8q24.1, is upregulated in 8q+ breast cancer and indicates poor clinical outcome in stage I and II disease. *Br J Cancer*. 2008;99(5):774–780. doi:10.1038/sj.bjc.6604556
- Mahoney CE, Pirman D, Chubukov V, et al. A chemical biology screen identifies a vulnerability of neuroendocrine cancer cells to SQLE inhibition. *Nat Commun*. 2019;10(1):96. doi:10.1038/s41467-018-07959-4
- Padyana AK, Gross S, Jin L, et al. Structure and inhibition mechanism of the catalytic domain of human squalene epoxidase. *Nat Commun*. 2019;10(1):97. doi:10.1038/s41467-018-07928-x
- Brown AJ, Chua NK, Yan N. The shape of human squalene epoxidase expands the arsenal against cancer. *Nat Commun*. 2019;10(1):888. doi:10.1038/s41467-019-08866-y
- Li Y, Ge D, Lu C. The SMART App: an interactive web application for comprehensive DNA methylation analysis and visualization. *Epigenetics Chromatin*. 2019;12(1):71. doi:10.1186/s13072-019-0316-3

23. Sun D, Wang J, Han Y, et al. TISCH: a comprehensive web resource enabling interactive single-cell transcriptome visualization of tumor microenvironment. *Nucleic Acids Res.* **2021**;49(D1):D1420–d1430. doi:10.1093/nar/gkaa1020
24. Luck K, Kim DK, Lambourne L, et al. A reference map of the human binary protein interactome. *Nature.* **2020**;580(7803):402–408. doi:10.1038/s41586-020-2188-x
25. Zhou Y, Zhou B, Pache L, et al. Metascape provides a biologist-oriented resource for the analysis of systems-level datasets. *Nat Commun.* **2019**;10(1):1523. doi:10.1038/s41467-019-09234-6
26. Vasaikar SV, Straub P, Wang J, Zhang B. LinkedOmics: analyzing multi-omics data within and across 32 cancer types. *Nucleic Acids Res.* **2018**;46(D1):D956. doi:10.1093/nar/gkx1090
27. Li T, Fu J, Zeng Z, et al. TIMER2.0 for analysis of tumor-infiltrating immune cells. *Nucleic Acids Res.* **2020**;48(W1):W509. doi:10.1093/nar/gkaa407
28. Jun SY, Brown AJ, Chua NK, et al. Reduction of Squalene Epoxidase by Cholesterol Accumulation Accelerates Colorectal Cancer Progression and Metastasis. *Gastroenterology.* **2020**;160(4):1194–1207.e28. doi:10.1053/j.gastro.2020.09.009
29. Garcia-Bermudez J, Baudrier L, Bayraktar EC, et al. Squalene accumulation in cholesterol auxotrophic lymphomas prevents oxidative cell death. *Nature.* **2019**;567(7746):118–122. doi:10.1038/s41586-019-0945-5
30. Kalyankrishna S, Grandis JR. Epidermal growth factor receptor biology in head and neck cancer. *J Clin Oncol.* **2006**;24(17):2666–2672. doi:10.1200/jco.2005.04.8306
31. Cruz JJ, Ocaña A, Del Barco E, Pandiella A. Targeting receptor tyrosine kinases and their signal transduction routes in head and neck cancer. *Ann Oncol.* **2007**;18(3):421–430. doi:10.1093/annonc/mdl175
32. Johnson DE. Targeting proliferation and survival pathways in head and neck cancer for therapeutic benefit. *Chin J Cancer.* **2012**;31(7):319–326. doi:10.5732/cjc.011.10404
33. Byeon HK, Ku M, Yang J. Beyond EGFR inhibition: multilateral combat strategies to stop the progression of head and neck cancer. *Exp Mol Med.* **2019**;51(1):1–14. doi:10.1038/s12276-018-0202-2
34. Murai T. Cholesterol lowering: role in cancer prevention and treatment. *Biol Chem.* **2015**;396(1):1–11. doi:10.1515/hsz-2014-0194
35. Silvente-Poirot S, Poirot M. Cholesterol metabolism and cancer: the good, the bad and the ugly. *Curr Opin Pharmacol.* **2012**;12(6):673–676. doi:10.1016/j.coph.2012.10.004
36. Chien MH, Lee TS, Kao C, Yang SF, Lee WS. Terbinafine inhibits oral squamous cell carcinoma growth through anti-cancer cell proliferation and anti-angiogenesis. *Mol Carcinog.* **2012**;51(5):389–399. doi:10.1002/mc.20800
37. Li B, Lu L, Zhong M, et al. Terbinafine inhibits KSR1 and suppresses Raf-MEK-ERK signaling in oral squamous cell carcinoma cells. *Neoplasma.* **2013**;60(4):406–412. doi:10.4149/neo\_2013\_052
38. Guo C, Chen S, Liu W, et al. Immunometabolism: a new target for improving cancer immunotherapy. *Adv Cancer Res.* **2019**;143:195–253. doi:10.1016/bs.acr.2019.03.004
39. Mazumdar C, Driggers EM, Turka LA. The Untapped Opportunity and Challenge of Immunometabolism: a New Paradigm for Drug Discovery. *Cell Metab.* **2020**;31(1):26–34. doi:10.1016/j.cmet.2019.11.014
40. Ho PC, Liu PS. Metabolic communication in tumors: a new layer of immunoregulation for immune evasion. *J Immunother Cancer.* **2016**;4:4. doi:10.1186/s40425-016-0109-1
41. Kaymak I, Williams KS, Cantor JR, Jones RG. Immunometabolic Interplay in the Tumor Microenvironment. *Cancer Cell.* **2021**;39(1):28–37. doi:10.1016/j.ccell.2020.09.004
42. Li X, Wenes M, Romero P, Huang SC, Fendt SM, Ho PC. Navigating metabolic pathways to enhance antitumour immunity and immunotherapy. *Nat Rev Clin Oncol.* **2019**;16(7):425–441. doi:10.1038/s41571-019-0203-7
43. Raccosta L, Fontana R, Corna G, Maggioni D, Moresco M, Russo V. Cholesterol metabolites and tumor microenvironment: the road towards clinical translation. *Cancer Immunol Immunother.* **2016**;65(1):111–117. doi:10.1007/s00262-015-1779-0
44. Zhang L, Romero P. Metabolic Control of CD8(+) T Cell Fate Decisions and Antitumor Immunity. *Trends Mol Med.* **2018**;24(1):30–48. doi:10.1016/j.molmed.2017.11.005
45. Ma X, Bi E, Huang C, et al. Cholesterol negatively regulates IL-9-producing CD8(+) T cell differentiation and antitumor activity. *J Exp Med.* **2018**;215(6):1555–1569. doi:10.1084/jem.20171576
46. Ma X, Bi E, Lu Y, et al. Cholesterol Induces CD8(+) T Cell Exhaustion in the Tumor Microenvironment. *Cell Metab.* **2019**;30(1):143–156. doi:10.1016/j.cmet.2019.04.002

## Cancer Management and Research

### Publish your work in this journal

Cancer Management and Research is an international, peer-reviewed open access journal focusing on cancer research and the optimal use of preventative and integrated treatment interventions to achieve improved outcomes, enhanced survival and quality of life for the cancer patient.

Submit your manuscript here: <https://www.dovepress.com/cancer-management-and-research-journal>

The manuscript management system is completely online and includes a very quick and fair peer-review system, which is all easy to use. Visit <http://www.dovepress.com/testimonials.php> to read real quotes from published authors.